

# Binding Motifs for Lanthanide Hydrides: A Combined Experimental and Theoretical Study of the $MH_x(H_2)_y$ Species ( $M = La-Gd$ ; $x = 1-4$ ; $y = 0-6$ )

Ivan Infante,<sup>†</sup> Laura Gagliardi,<sup>\*,†</sup> Xuefeng Wang,<sup>‡</sup> and Lester Andrews<sup>\*,‡</sup>

Department of Physical Chemistry, University of Geneva, 30 Quai Ernest Ansermet, CH-1211 Geneva, Switzerland, and Department of Chemistry, University of Virginia, Charlottesville, Virginia 22904-4319

Received: November 12, 2008; Revised Manuscript Received: December 23, 2008

The results of a combined spectroscopic and computational study of lanthanide hydrides with the general formula  $MH_x(H_2)_y$ , where  $M = La, Ce, Pr, Nd, Sm, Eu, \text{ and } Gd$ ,  $x = 1-4$ , and  $y = 0-6$  are reported. To understand the nature of the dihydrogen complexes formed with lanthanide metal hydride molecules, we have first identified the binary  $MH_x$  species formed in the ablation/deposition process and then analyzed the dihydrogen supercomplexes,  $MH_x(H_2)_y$ . Our investigation shows that the trihydrides bind dihydrogen more weakly than the dihydrides and that the interaction between the central lanthanide and the  $H_2$  molecules occurs via a 6s electron transfer from the lanthanide to the  $H_2$  molecules. Evidence is also presented for the  $SmH$  and  $EuH$  diatomic molecules and the tetrahydride anions in solid hydrogen.

## Introduction

An ideal chemical hydrogen storage material has a low molar weight, is inexpensive, has rapid kinetics for absorbing and desorbing  $H_2$ , and stores large quantities of hydrogen reversibly. Under these conditions, metal hydrides are of considerable interest because they, in principle, meet these requirements.<sup>1</sup> The challenge of finding suitable candidates also poses another question that is more pedagogical but equally fascinating: what is the maximum number of hydrogen atoms that a metal can bind?

Both theory and experiment play a major role in attempting to answer this question. In this contribution, we combine matrix infrared spectroscopy measurement and density functional calculations to achieve an understanding of the bonding between a metal and the hydrogen atoms.

The coordination of dihydrogen to metals has attracted considerable attention since the Kubas tungsten complexes were first discovered.<sup>2-4</sup> The metal hydride species, prepared with laser-ablated metal atoms and hydrogen, show two types of hydrogen-metal interactions, a direct  $\sigma$  metal hydride bond, in which the hydrogen shares its 1s electron with one of the available valence electrons of the metal, and a side-on type of bond, in which a dihydrogen molecule is “complexed” to the metal. The former is obviously the stronger kind and can give rise to four basic hydride species:  $MH$ ,  $MH_2$ ,  $MH_3$ , and  $MH_4$ . The latter bond will form a complex of type  $MH_x(H_2)_y$  ( $x = 1-4$ ;  $y = 0-6$ ), in which the number of hydrogen atoms attached to it in the first shell,  $x$ , or hydrogen molecules in the second shell or side-bound ligand layer,  $y$ , will depend on the properties of the metal atom involved.

Infrared spectroscopic measurements for several metal compounds have been performed in noble gas matrices, and comprehensive works have been performed on lanthanide and group III metals.<sup>5,6</sup> However, performing these reactions in pure hydrogen will give a higher product yield and larger complexes

and will provide further insight into the metal-hydrogen bond. Recently, we have reported the  $WH_4(H_2)_4$  and  $ThH_4(H_2)_4$  species using infrared spectroscopy and density functional theory (DFT) to identify the strongest vibrational frequencies and isotopic shifts of this complex.<sup>7-9</sup> The formation of  $UH_4(H_2)_6$  has also been proposed,<sup>10</sup> which represents a record for the number of hydrogen atoms that can be bound to a metal.

In this investigation, we present the results of a systematic study of lanthanide hydrides with the general formula  $MH_x(H_2)_y$ , where  $M = La, Ce, Pr, Nd, Sm, Eu, \text{ and } Gd$ ,  $x = 1-4$ , and  $y = 0-6$ . Comparative calculations were also performed on the species in which the central metal,  $M$ , is  $Mo, W, \text{ and } U$ . Earlier investigations from one of our laboratories focused on infrared spectra of these binary metal hydrides in solid argon.<sup>11-13</sup> Most germane to the present work is our early comprehensive report of lanthanide metal hydride molecules.<sup>5</sup> With the support of electronic structure calculations, we can better predict the nature of the metal-hydrogen interactions and which system presents the largest number of hydrogen molecules bonded to the central metal.

## Computational and Experimental Methods

Quantum chemical calculations were performed using DFT. The TURBOMOLE package was employed.<sup>14</sup> Scalar relativistic effects were incorporated by employing on the lanthanide metal atoms the Stuttgart RSC Segmented/ECP basis set with 28 core electrons and contraction of  $(14s13p10d8f3g)/[10s8p5d4f3g]$  type.<sup>15</sup> A valence triple- $\zeta$  split valence basis set, TZVPP, was used on the hydrogen atoms. The gradient-corrected BP86 exchange correlation (xc) functional was employed. Some of the calculations were also repeated using the PBE<sup>16</sup> and PBE0 xc functionals.<sup>17</sup> Full geometry optimizations, frequency calculations, and assessment of the correct ground-state spin multiplicity were performed for all species. Basis set superposition error (BSSE) corrections were included using the counterpoise method. Zero-point energy corrections (ZPE) were also computed.

We have studied the interaction between the hydrogen atoms and the metal by classifying the energy of the  $MH_x$  systems in

\* Corresponding authors. E-mail: laura.gagliardi@chiph.unige.ch (L.G.), isa@virginia.edu (L.A.).

<sup>†</sup> University of Geneva and University of Minnesota.

<sup>‡</sup> University of Virginia.

a series of contributions. The bonding energy,  $\Delta E_{\text{bond}}$ , between two fragments is expressed as the sum of two terms: one destabilizing term called strain energy or preparation energy,  $\Delta E_{\text{strain}}$  (the two expressions will be used as synonyms in the following), and one stabilizing term called interaction energy,  $\Delta E_{\text{int}}$  ( $\Delta E_{\text{bond}} = \Delta E_{\text{strain}} + \Delta E_{\text{int}}$ ).  $\Delta E_{\text{strain}}$  is associated with the deformation of the individual fragments when they form the supersystem. This contribution is always positive, and its magnitude depends on the rigidity and reorganization of each fragment.  $\Delta E_{\text{int}}$  is the effective interaction between the deformed fragments. This procedure has shown to be very informative for similar systems.<sup>18–20</sup> To analyze the charge transfer between the metal and the hydrogen moieties, we used the natural population charges as implemented in TURBOMOLE.

The experiment for reactions of laser-ablated lanthanide metal atoms with hydrogen molecules during condensation at 4 K has been previously described in detail.<sup>21</sup> The Nd/YAG laser fundamental (1064 nm, 10 Hz repetition rate with 10 ns pulse width) was focused onto a rotating metal target (Johnson–Matthey). The laser energy was varied from 1 to 10 mJ/pulse. Laser-ablated lanthanide metal atoms were codeposited with 3 to 4 mmol of normal or *para*-hydrogen<sup>22,23</sup> molecules onto a 4 K CsI cryogenic window for 30 min using a Sumitomo Heavy Industries Model RDK-205D cryocooler. Hydrogen (Matheson), D<sub>2</sub>, and HD (Cambridge Isotopic Laboratories) were used in different experiments. FTIR spectra were recorded at 0.5 cm<sup>-1</sup> resolution on a Nicolet 750 apparatus with 0.1 cm<sup>-1</sup> accuracy using a HgCdTe range B detector. Matrix samples were annealed at different temperatures, and selected samples were subjected to broadband photolysis by a medium-pressure mercury arc lamp (Philips, 175W) with the outer globe removed.

## Results and Discussion

DFT-based calculations were initially performed to optimize the structures of all possible  $\text{MH}_x(\text{H}_2)_y$  species and to determine the interaction energy of the classical  $\text{MH}_x$  with several dihydrogen molecules. Solid hydrogen matrix infrared spectroscopy was then used to provide “matrix shifts” in the guest molecule frequencies and uncertainties in the number of complexing dihydrogen ligands associated with a particular binary lanthanide metal hydride core molecule. With the interplay of the two approaches, we were able to provide new spectroscopic and computational information for such difficult metal hydride systems and to find a consistent model to explain the properties of these new dihydrogen complexes.

**Structure and Energetics.** The metal–hydrogen bond distances for several metal hydrides are reported in Table 1. For a given structure, two kinds of M–H bonds were considered, namely, M–H<sup>1</sup> for the  $\sigma$ -bonded hydrogen atoms (the classical hydrides) and M–H<sup>2</sup> for the bond with a H<sub>2</sub> molecule (a dihydrogen ligand). The values reported in Table 1 have been averaged over all possible M–H<sup>1</sup> and M–H<sup>2</sup> bond distances for a particular  $\text{MH}_x(\text{H}_2)_y$  species [ $x = 2, 3, 4$ ;  $y = 0–6$ ]. In Table 2, we report the spin multiplicities for the electronic ground state of all of the species reported in Table 1.

We decided to proceed in a multistep way by adding one hydrogen molecule at a time to the  $\text{MH}_x$  classical hydride and allowing a full geometry optimization for each cluster. This approach should, in principle, be representative of what happens experimentally when the hydrogen molecules bond one after the other to the  $\text{MH}_x$  molecules produced in the laser-ablated and excited metal atom reactions. Computationally, we compare the total energy (including ZPE) of the  $\text{MH}_4(\text{H}_2)_y$  and  $\text{MH}_2(\text{H}_2)_{y+1}$  clusters to decide which of the two types is more

**TABLE 1: Typical Bond Metal Hydride and Metal Dihydrogen Distances (Å) for Various Ground-State Species of  $\text{MH}_2(\text{H}_2)_y$ ,  $\text{MH}_3(\text{H}_2)_y$ , and  $\text{MH}_4(\text{H}_2)_y$  Computed at DFT/BP86/TZVPP Level of Theory<sup>a</sup>**

|                 | MH <sub>2</sub>                                    | La                  | Ce                 | Pr   | Nd   | Sm   | Eu   | Gd   |
|-----------------|--|---------------------|--------------------|--|------|------|------|------|
| y = 0           | 2.14   |                     | 2.07               | 2.09   | 2.10 | 2.11 | 2.11 | 2.04 |
| y = 1           | 2.11   |                     | 2.08               | 2.10   | 2.11 | 2.11 | 2.11 | 2.05 |
|                 | 2.38   |                     | 2.31               | 2.37   | 2.44 | 2.57 | 2.67 | 2.45 |
| y = 2           | 2.13   |                     | 2.08               | 2.10   | 2.09 | 2.12 | 2.12 | 2.05 |
|                 | 2.46   |                     | 2.42               | 2.49   | 2.53 | 2.50 | 2.47 | 2.49 |
| y = 3           | 2.14   |                     | 2.08               | 2.09   | 2.12 | 2.13 | 2.13 | 2.06 |
|                 | 2.47   |                     | 2.42               | 2.43   | 2.47 | 2.46 | 2.43 | 2.55 |
| y = 4           | 2.14   |                     | 2.09               | 2.11   | 2.13 | 2.13 | 2.13 |      |
|                 | 2.46   |                     | 2.43               | 2.41   | 2.45 | 2.46 | 2.48 |      |
| y = 5           | 2.15   |                     | 2.09               | 2.12   | 2.12 | 2.13 | 2.14 |      |
|                 | 2.48   |                     | 2.42               | 2.44   | 2.43 | 2.48 | 2.48 |      |
| y = 6           | 2.15   |                     | 2.10               | 2.11   | 2.12 | 2.13 | 2.15 |      |
|                 | 2.49   |                     | 2.43               | 2.44   | 2.45 | 2.47 | 2.48 |      |
| MH <sub>3</sub> | La   | Ce                  | Pr                 | Nd   | Sm   | Eu   | Gd   |      |
| y = 0           | 2.12   | 2.06                | 2.05               | 2.06   | 2.09 | 2.10 | 2.01 |      |
| y = 1           | 2.13   | 2.06                | 2.05               | 2.04   | 2.07 | 2.10 | 2.03 |      |
|                 | 2.40   | 2.33                | 2.29               | 2.26   | 2.25 | 2.32 | 2.45 |      |
| y = 2           | 2.13   | 2.07                | 2.05               | 2.04   | 2.06 | 2.11 | 2.03 |      |
|                 | 2.42   | 2.34                | 2.31               | 2.29   | 2.30 | 2.27 | 2.46 |      |
| y = 3           | 2.14   | 2.07                | 2.06               | 2.04   | 2.07 | 2.12 | 2.04 |      |
|                 | 2.43   | 2.36                | 2.34               | 2.32   | 2.34 | 2.34 | 2.47 |      |
| y = 4           | 2.14   | 2.08                | 2.06               | 2.05   | 2.07 | 2.12 | 2.04 |      |
|                 | 2.45   | 2.40                | 2.37               | 2.36   | 2.39 | 2.38 | 2.54 |      |
| y = 5           | 2.16   | 2.09                | 2.07               | 2.06   | 2.07 | 2.12 |      |      |
|                 | 2.48   | 2.42                | 2.40               | 2.37   | 2.40 | 2.41 |      |      |
| y = 6           | 2.16   | 2.10                | 2.08               | 2.07   | 2.08 | 2.12 |      |      |
|                 | 2.50   | 2.45                | 2.42               | 2.40   | 2.39 | 2.43 |      |      |
| MH <sub>4</sub> | Cr   | Mo                  | W                  | Nd   | U    |      |      |      |
| y = 1           | 1.64   | 1.64                | 1.67               | 2.11   | 2.01 |      |      |      |
|                 | 1.95   | 1.69                | 1.71               | 2.44   | 2.19 |      |      |      |
|                 | as CrH <sub>2</sub> (H <sub>2</sub> )              |                     |                    | as NdH <sub>2</sub> (H <sub>2</sub> )              |      |      |      |      |
| y = 2           | 1.66   | 1.66                | 1.69               | 2.11   | 2.01 |      |      |      |
|                 | 1.91   | as MoH <sub>6</sub> | as WH <sub>6</sub> | 2.44   | 2.24 |      |      |      |
|                 | as CrH <sub>2</sub> (H <sub>2</sub> ) <sub>2</sub> |                     |                    | as NdH <sub>2</sub> (H <sub>2</sub> )              |      |      |      |      |
| y = 3           | 1.61   | 1.71                | 1.72               | 2.11   | 2.01 |      |      |      |
|                 | 1.71   | 1.81                | 1.86               | 2.44   | 2.27 |      |      |      |
|                 | as CrH <sub>2</sub> (H <sub>2</sub> ) <sub>3</sub> |                     |                    | as NdH <sub>2</sub> (H <sub>2</sub> ) <sub>2</sub> |      |      |      |      |
| y = 4           | 1.67   | 1.72                | 1.74               | 2.13   | 2.02 |      |      |      |
|                 | as Cr(H <sub>2</sub> ) <sub>5</sub>                | 1.83                | 1.85               | 2.45   | 2.31 |      |      |      |
|                 |  |                     |                    | as NdH <sub>2</sub> (H <sub>2</sub> ) <sub>2</sub> |      |      |      |      |
| y = 5           | 1.67   |                     |                    | 2.12   | 2.02 |      |      |      |
|                 | as Cr(H <sub>2</sub> ) <sub>6</sub>                |                     |                    | 2.43   | 2.32 |      |      |      |
|                 |  |                     |                    | as NdH <sub>2</sub> (H <sub>2</sub> ) <sub>2</sub> |      |      |      |      |
| y = 6           |  |                     |                    | 2.12   | 2.03 |      |      |      |
|                 |  |                     |                    | 2.45   | 2.34 |      |      |      |
|                 |  |                     |                    | as NdH <sub>2</sub> (H <sub>2</sub> ) <sub>2</sub> |      |      |      |      |

<sup>a</sup> In the case of Cr, more than one H<sub>2</sub> molecule is attached to the metal, and thus the supercomplex transforms first into CrH<sub>2</sub>(H<sub>2</sub>)<sub>y</sub> for  $y < 3$  and then into Cr(H<sub>2</sub>)<sub>y</sub>. As for the Nd species, the NdH<sub>2</sub>(H<sub>2</sub>)<sub>y</sub> is always less stable than its NdH<sub>2</sub>(H<sub>2</sub>)<sub>y+1</sub> isomer and in most cases does not form a stable minimum (i.e., no imaginary frequencies) or is found at much higher energies, hence we do not consider it here.

stable and is thus likely to be formed in the matrix. We assume that both types of clusters have the same kinetics of absorbing H<sub>2</sub> molecules. Even if most lanthanides are strongly trivalent, for the  $\text{MH}_3(\text{H}_2)_y$  species, such energy comparisons are more difficult because of the different stoichiometry. However, excess energy is available in the laser-ablation process, and the  $\text{MH}_3$  species can be formed through the reaction of MH and H<sub>2</sub> molecules or H atoms and  $\text{MH}_2$  molecules.

The calculations indicate that with the exception of cerium, most of the lanthanides preferentially form the  $\text{MH}_2(\text{H}_2)_{y+1}$  species rather than the  $\text{MH}_4(\text{H}_2)_y$  compounds, especially when  $y$  is equal to 1, 2, and 3. Some compounds, like  $\text{MH}_4(\text{H}_2)_4$  ( $M = \text{Pr}, \text{Nd}$ ), have been successfully optimized, and they present all real frequencies. However, they are less likely to form experimentally. This interpretation finds confirmation in Table

**TABLE 2: Spin Multiplicities for Each of the Electronic Ground-State Species Optimized At DFT/BP86/TZVPP Level of Theory<sup>a</sup>**

|  | La  | Ce                             | Pr                            | Nd   | Sm      | Eu     | Gd    |
|--|---|--------------------------------|-------------------------------|--|---------|--------|-------|
| MH   | singlet   | doublet                        | triplet                       | sextet   | octet   | nonet  | octet |
| MH <sub>2</sub>  | doublet   | triplet                        | quartet                       | quintet  | septet  | octet  | nonet |
| MH <sub>3</sub>  | singlet   | doublet                        | triplet                       | quartet  | sextet  | septet | octet |
| MH <sub>4</sub>  | doublet   | singlet                        | doublet                       | triplet  | quintet | sextet | nonet |
| MH <sub>4</sub> <sup>-</sup>                                   | singlet   | doublet                        | triplet                       | quartet  | sextet  | septet | octet |
| MH <sub>2</sub> (H <sub>2</sub> ) <sub>y</sub> [y = 1, ..., 6] | doublet   | triplet                        | quartet                       | quintet  | septet  | octet  | nonet |
| MH <sub>3</sub> (H <sub>2</sub> ) <sub>y</sub> [y = 1, ..., 6] | singlet   | doublet                        | triplet                       | quartet  | sextet  | septet | octet |
|  | Cr  | Mo                             | W                             | Nd   | U       |        |       |
| MH <sub>2</sub>  | quintet   | quintet                        | quintet                       | quintet  | quintet |        |       |
| MH <sub>4</sub>  | quintet as CrH <sub>2</sub> (H <sub>2</sub> )                 | triplet                        | triplet                       | triplet  | triplet |        |       |
| MH <sub>4</sub> (H <sub>2</sub> )                              | quintet<br>as CrH <sub>2</sub> (H <sub>2</sub> ) <sub>2</sub> | singlet<br>as MoH <sub>6</sub> | singlet<br>as WH <sub>6</sub> | quintet<br>as MH <sub>2</sub> (H <sub>2</sub> ) <sub>2</sub> | triplet |        |       |
| MH <sub>4</sub> (H <sub>2</sub> ) <sub>2</sub>                 | quintet<br>as CrH <sub>2</sub> (H <sub>2</sub> ) <sub>3</sub> | singlet                        | singlet                       | quintet<br>as MH <sub>2</sub> (H <sub>2</sub> ) <sub>3</sub> | triplet |        |       |
| MH <sub>4</sub> (H <sub>2</sub> ) <sub>3</sub>                 | singlet<br>as Cr(H <sub>2</sub> ) <sub>5</sub>                | singlet                        | singlet                       | quintet<br>as MH <sub>2</sub> (H <sub>2</sub> ) <sub>4</sub> | triplet |        |       |
| MH <sub>4</sub> (H <sub>2</sub> ) <sub>4</sub>                 | singlet<br>as Cr(H <sub>2</sub> ) <sub>6</sub>                | singlet                        | singlet                       | quintet<br>as MH <sub>2</sub> (H <sub>2</sub> ) <sub>5</sub> | triplet |        |       |

<sup>a</sup> All of the relevant structures are presented. For the group VI elements, we report only the species with an even number of hydrogen atoms because the oddly numbered species are not met in the experimental conditions.

**TABLE 3: Energy Differences (kcal/mol) between MH<sub>4</sub> and Other Isomeric Species with M = La, Ce, Pr, Nd, Sm, Eu, Gd, Cr, Mo, W, and U computed at DFT/BP86/TZVPP Level of Theory<sup>a</sup>**

|  | La             | Ce               | Pr               | Nd             | Sm               | Eu             | Gd               |
|--|----------------|------------------|------------------|----------------|------------------|----------------|------------------|
| E[MH <sub>4</sub> ]-E[MH <sub>2</sub> (H <sub>2</sub> )]   | 31.5<br>(26.5) | 12.2<br>(9.6)    | 35.5<br>(31.7)   | 46.9<br>(42.9) | 56.8<br>(52.4)   | 64.5<br>(60.4) | 3.3<br>(3.3)     |
| E[MH <sub>4</sub> ]-E[M(H <sub>2</sub> ) <sub>2</sub> ]    | 15.7<br>(8.6)  | -6.9<br>(-10.9)  | 19.0<br>(15.2)   | 29.9<br>(23.9) | 42.9<br>(36.5)   | 71.9<br>(68.1) | -15.9<br>(-17.6) |
| E[MH <sub>4</sub> ]-E[MH <sub>2</sub> ]-E[H <sub>2</sub> ] | 18.6<br>(17.1) | 7.6<br>(-8.3)    | 32.1<br>(31.5)   | 43.2<br>(42.1) | 54.3<br>(52.6)   | 63.1<br>(61.3) | 0.4<br>(3.5)     |
|  | Cr             | Mo               | W                | Nd             | U                |                |                  |
| E[MH <sub>4</sub> ]-E[MH <sub>2</sub> (H <sub>2</sub> )]   | 16.4<br>(15.6) | -13.1<br>(-13.3) | -24.6<br>(-24.7) | 46.9<br>(42.9) | -9.5<br>(-10.9)  |                |                  |
| E[MH <sub>4</sub> ]-E[M(H <sub>2</sub> ) <sub>2</sub> ]    | 2.3<br>(1.3)   | -22.6<br>(-23.8) | -44.4<br>(-44.0) | 29.9<br>(23.9) | -31.1<br>(-34.2) |                |                  |
| E[MH <sub>4</sub> ]-E[MH <sub>2</sub> ]-E[H <sub>2</sub> ] | 10.8<br>(13.3) | -19.5<br>(-16.7) | -32.6<br>(-29.7) | 43.2<br>(42.1) | -12.6<br>(-11.4) |                |                  |

<sup>a</sup> A negative value means that the MH<sub>4</sub> is the most stable conformer. In parentheses, values including the zero-point energy correction are reported.

3, where we compared the stability (including ZPE) of MH<sub>4</sub> to that of MH<sub>2</sub>(H<sub>2</sub>) and M(H<sub>2</sub>)<sub>2</sub>. It is evident that the MH<sub>4</sub> fragment is thermodynamically less stable than, for example, MH<sub>2</sub>(H<sub>2</sub>). The only exception is represented by cerium, for which the energy difference between MH<sub>4</sub> and MH<sub>2</sub>(H<sub>2</sub>) is not very large (about 10 kcal/mol), and we were able to compute all types of complexes. This result is also confirmed by a previous laser ablation experiment using argon as the trapping material, where traces of CeH<sub>4</sub> have been identified.<sup>5</sup>

In the middle of the row, the gadolinium classical hydride GdH<sub>2</sub> binds only weakly to any H<sub>2</sub> molecule. Without the inclusion of the ZPE, the formation of the supercomplexes is slightly favorable, whereas with ZPE, the reactants (i.e., the separate fragments) are more stable of about 1 to 3 kcal/mol. However, the latter result may very well be a flaw of the calculations because the error in the DFT interaction energies can be larger than these small values. Therefore, because experimentally weak bands of supercomplexes of gadolinium are visible, we assume that the interaction exists, even if it is very small.

For samarium and europium, the formation of MH<sub>2</sub>(H<sub>2</sub>)<sub>x</sub> with x = 1, 2, 3 is also hindered from a computational standpoint,

and this would suggest that the heavier lanthanides Sm, Eu, and Gd would not form any supermolecular reaction products with an even number of hydrogen atoms. However, as in the case of Gd, the presence of weak bands of supercomplexes in the spectra suggests the formation of a bonding interaction, even though it is weak.

The MH<sub>3</sub> fragments are also more favorable to the complexation with H<sub>2</sub> molecules in the case of M = Sm, Eu, and Gd, thus indicating that these lanthanide species could also form stable agglomerates.

For the compounds of group VI elements (Cr, Mo, W) and uranium, the situation is different. Chromium preferentially forms the CrH<sub>2</sub>(H<sub>2</sub>)<sub>y</sub> systems with y up to 3. For y > 3, the Cr(H<sub>2</sub>)<sub>y+1</sub> clusters are more stable than the CrH<sub>2</sub>(H<sub>2</sub>)<sub>y</sub> clusters. An inspection of Table 3 shows that Mo, W, and U largely favor the MH<sub>4</sub> species (with respect to MH<sub>2</sub>(H<sub>2</sub>), M(H<sub>2</sub>)<sub>2</sub>), and for these elements, we decided to study mainly the MH<sub>4</sub>(H<sub>2</sub>)<sub>y</sub> supermolecules because of the clear experimental evidence of the dominating presence of these species in the vibrational spectra.<sup>11-13</sup>

In Figure 1a,b, we report the energy difference  $E[\text{MH}_2(\text{H}_2)_y] - E[\text{MH}_2] - yE[\text{H}_2]$  versus the number, y, of H<sub>2</sub> molecules

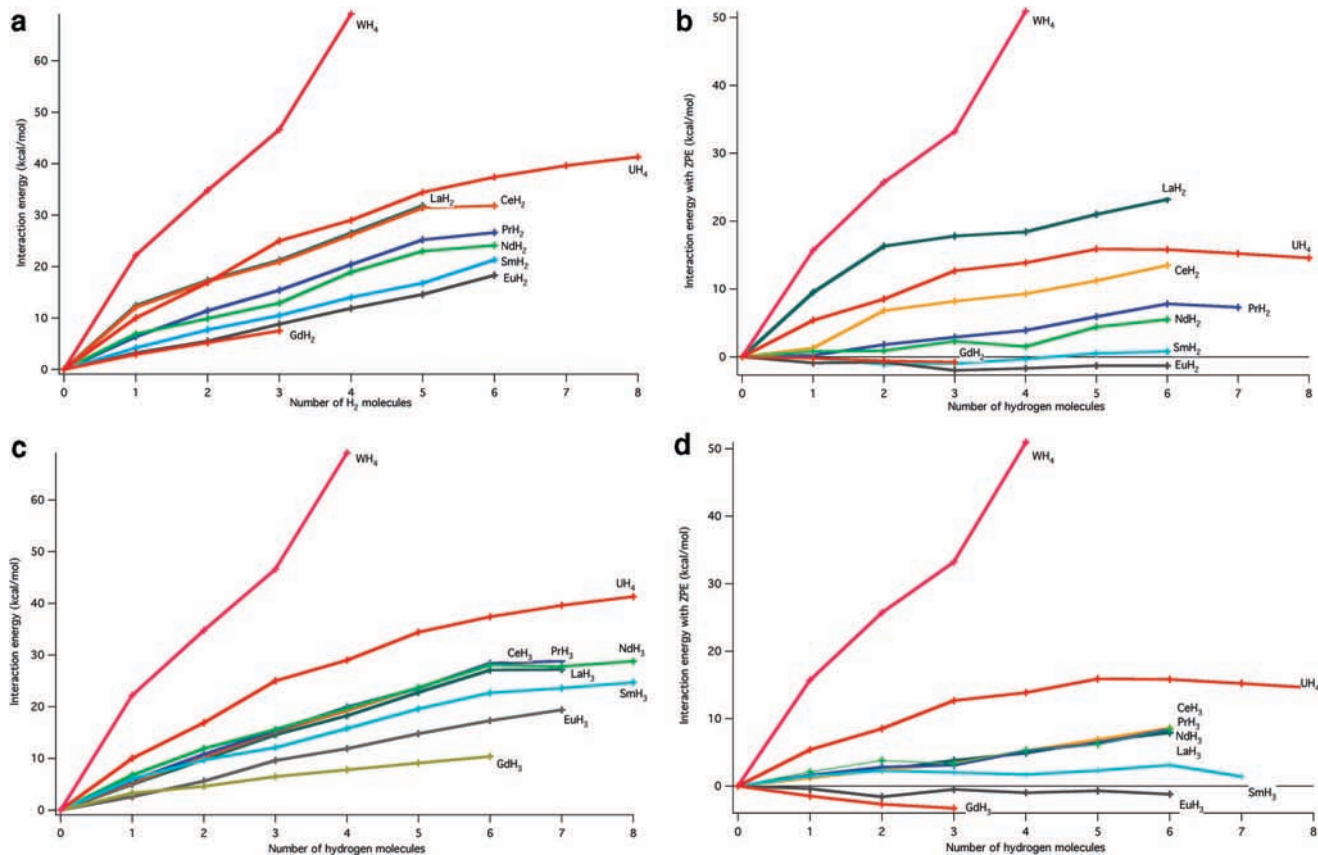


**Figure 1.** Energy difference  $E[\text{MH}_x(\text{H}_2)_y] - E[\text{MH}_x] - yE[\text{H}_2]$  [ $x = 2, 3$ ] versus the number,  $y$ , of  $\text{H}_2$  molecules (a,c) without ZPE corrections and (b,d) with the ZPE correction. All values were computed at DFT/BP86/TZVPP level of theory. The BSSE effect, around 1 to 2 kcal/mol, is not included.

without and with the ZPE correction, respectively. In Figure 1c,d we report the energy difference  $E[\text{MH}_3(\text{H}_2)_y] - E[\text{MH}_3] - yE[\text{H}_2]$  versus the number,  $y$ , of  $\text{H}_2$  molecules without and with the ZPE correction, respectively. The stability of the W and U clusters is also reported for comparison. Because of the choice of a large basis set, the BSSE effects (benchmarked only on selected species) on the energy differences are reasonably small, around 1 to 2 kcal/mol. This value is smaller than the energy gain obtained by adding  $\text{H}_2$  for small values of  $y$ , but it becomes of the same order of magnitude when  $y$  is larger than 6. This suggests that the energy gain for  $y > 6$  shown in Figure 1a,c may not actually occur. Furthermore, Figure 1b,d, where the ZPE corrections have been added, show that the interaction energies are drastically reduced for all elements and that some species such as  $\text{SmH}_2(\text{H}_2)_x$  and  $\text{EuH}_2(\text{H}_2)_x$  have negative values, indicating a disproportioning of the supercomplex  $\text{MH}_2(\text{H}_2)_x$  to the isolated fragments. A similar pattern is found for the  $\text{MH}_3(\text{H}_2)_x$  species. However, these negative values are of the same order of magnitude as the approximations used in the calculations. Indeed, we have observed  $\text{SmH}_2$  and  $\text{EuH}_2$  in solid hydrogen, but the interaction with extra  $\text{H}_2$  could be weak, as the DFT results suggest. Therefore, we can just obtain these molecules trapped in solid hydrogen without forming stable complexes with more  $\text{H}_2$  molecules.

Regarding the group VI series and uranium, the striking feature remains the much larger stabilization energy of  $\text{MoH}_4(\text{H}_2)_y$  and  $\text{WH}_4(\text{H}_2)_y$  upon the addition of  $\text{H}_2$  molecules. For  $y = 4$ , which is the maximum  $y$  (number of  $\text{H}_2$  molecules) reachable for these complexes, the interaction energy with the  $\text{H}_2$  molecules is at least three times larger than that for the lanthanide atoms.  $\text{UH}_4$  has a stabilization energy of about 25

kcal/mol, which is larger than that in the  $\text{NdH}_4$  case but smaller compared with the 65 kcal/mol of  $\text{WH}_4$ . Despite the smaller interaction energy,  $\text{UH}_4$  has enough space to accommodate up to five or six  $\text{H}_2$  molecules.

Summarizing our calculations, among all of the possible lanthanide  $\text{MH}_x$  classical hydrides, the only ones that may form stable supercomplexes of  $\text{MH}_x(\text{H}_2)_y$  type are La, Ce, Pr, and Nd. Among these, only Cerium shows the formation of tetravalent  $\text{CeH}_4(\text{H}_2)_y$  hydrides, whereas the others can form only divalent  $\text{MH}_2(\text{H}_2)_y$  or trivalent  $\text{MH}_3(\text{H}_2)_y$  hydrides. All elements could form stable basic  $\text{MH}_x$  (with  $x = 2, 3, 4$ ) components with no  $\text{H}_2$  molecules attached. Only weak interactions can be obtained for Sm, Eu, and Gd, but they are strong enough to be identified as weak bands in the experimental spectra. For elements of group VI, chromium mainly forms aggregates of  $\text{CrH}_2(\text{H}_2)_y$  type or  $\text{Cr}(\text{H}_2)_{y+1}$  for  $y > 3$ , whereas Mo, W, and U form supercomplexes of  $\text{MH}_4(\text{H}_2)_y$  type only. Among all of these combinations of supercomplexes, the maximum number of hydrogen atoms that can be attached to a metal is 14 to 15, a value achieved by La, Ce, Pr, Nd, and U. Uranium can probably also form the species  $\text{UH}_4(\text{H}_2)_6$  with 16 hydrogens in all. In the Ln compounds, as in the group VI, U, and Nd compounds, the H–H bond distance of the  $\text{H}_2$  moieties significantly elongates (about 0.80 Å, see the Supporting Information). In Figure 2a,b, the structures for  $\text{MH}_4(\text{H}_2)_4$  in which the metal is a lanthanide atom or a group VI atom, such as tungsten, are reported, respectively.

**Infrared Spectra.** Infrared spectra were recorded from samples prepared by codepositing laser-ablated early lanthanide metal atoms and normal hydrogen at 4 K. These spectra contain bands due to solid hydrogen and the trapped hydride anion as

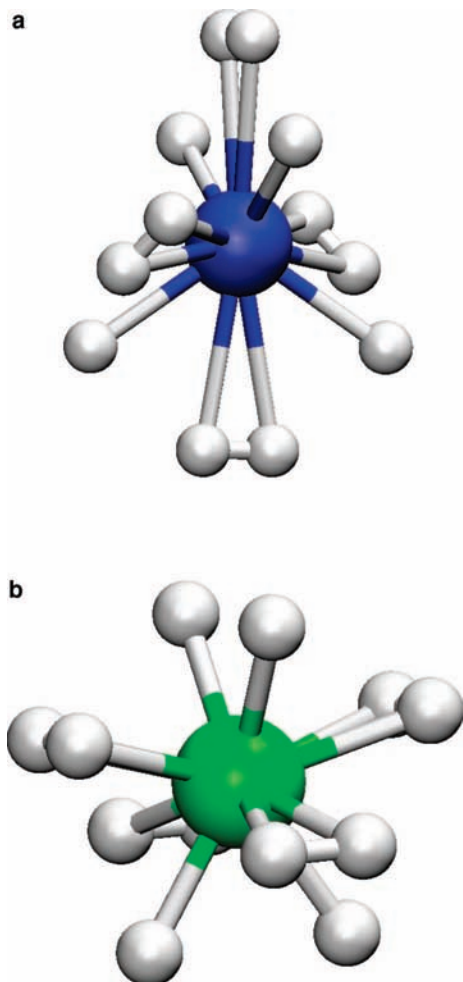


**Figure 2.** Structures for  $MH_4(H_2)_4$  in which the metal is (a) a lanthanide atom or (b) a group VI atom, such as tungsten. A different type of bonding occurs with the peripheral  $H_2$  molecules.

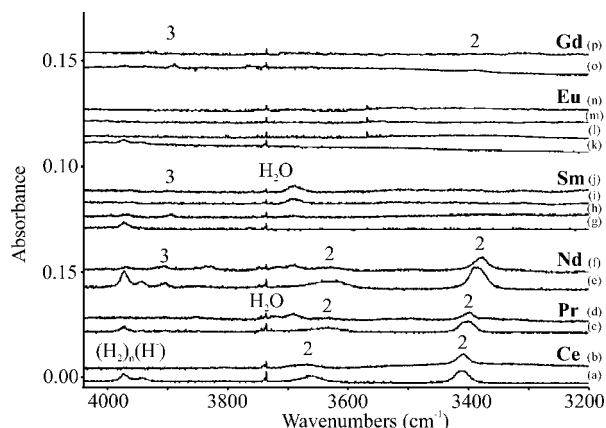


**Figure 3.** Infrared spectra for the products of reaction of early lanthanide metal atoms with dihydrogen during co-condensation at 4 K. (a) Ce codeposition, (b) after  $>290$  nm irradiation; (c) Pr codeposition, (d) after 240–380 nm irradiation; (e) Nd codeposition, (f) after 240–380 nm irradiation; (g) Sm codeposition, (h) after  $>470$  nm irradiation, (i) after 240–380 nm irradiation, and (j) after  $>530$  nm irradiation; (k) Eu codeposition, (l) after  $>470$  nm irradiation, (m) after  $>380$  nm irradiation, and (n) after 240–380 nm irradiation; and (o) Gd codeposition, (p) after  $>320$  nm irradiation.

it perturbs the surrounding dihydrogen ligands.<sup>24</sup> Infrared spectra of the important new absorptions are shown in Figures 3 and 4 for the H–H and Ln–H stretching regions. To understand the dihydrogen complexes formed with lanthanide metal hydride

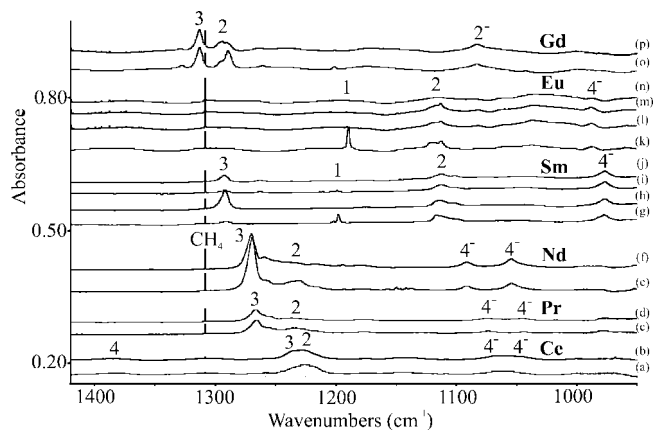


**Figure 4.** Infrared spectra for the products of reaction of early lanthanide metal atoms with dihydrogen during co-condensation at 4 K. (a) Ce codeposition, (b) after  $>290$  nm irradiation; (c) Pr codeposition, (d) after 240–380 nm irradiation; (e) Nd codeposition, (f) after 240–380 nm irradiation; (g) Sm codeposition, (h) after  $>470$  nm irradiation, (i) after 240–380 nm irradiation, and (j) after  $>530$  nm irradiation; (k) Eu codeposition, (l) after  $>470$  nm irradiation, (m) after  $>380$  nm irradiation, and (n) after 240–380 nm irradiation; and (o) Gd codeposition, (p) after  $>320$  nm irradiation.

molecules, we first need to identify the binary  $LnH_x$  molecule formed in the ablation/deposition process, which becomes the core in the dihydrogen supercomplex. To this end, we compare spectra in the Ln–H stretching region where product bands are labeled with small numbers ( $x$ ), which indicate the number of classical hydrides on the metal center, that is,  $LnH_x$ . This  $LnH_x$  molecule forms the core of a larger dihydrogen complex,  $LnH_x(H_2)_y$ , which is the subject of our investigation.

Notice first that there is a single band labeled 4 (Figure 4a). In the case of Ce, we believe that this weak  $1381\text{ cm}^{-1}$  absorption is due to  $CeH_4(H_2)_y$ , because isolated  $CeH_4$  in solid argon was assigned at  $1442\text{ cm}^{-1}$ .<sup>5</sup> Next, realize that the spectra are dominated by bands labeled 3 with the notable exception of spectra recorded after Eu reactions (k–n). These bands labeled 3 correlate reasonably well with the calculated position of the strongest absorptions for the corresponding  $LnH_3(H_2)_y$  complexes, including the failure to converge a stable  $EuH_3$  molecule. The  $LnH + H_2$  reaction energies provide some measure of how favorable the  $LnH_3$  product is in these experiments, and we note that  $EuH_3$  has the highest endothermic value (+29 kcal/mol) and  $CeH_3$  is the most exothermic (–24 kcal/mol). It is important that we have mixed isotopic spectra from experiments with pure HD that convincingly identify the gadolinium dihydride and trihydride core molecules (Figure 5). First, the  $GdH_2$  absorptions at  $1327.2$  and  $1289.1\text{ cm}^{-1}$  are near our computed  $1330$  and  $1268\text{ cm}^{-1}$  values for the  $GdH_2$  molecule in the nonet ground state but lower than the solid argon values of  $1399.0$  and  $1359.3\text{ cm}^{-1}$ .<sup>5</sup> The single intermediate band at  $1307.0\text{ cm}^{-1}$  is then due to  $GdHD$  for this core molecule with two equivalent H(D) atoms. Notice that some  $GdH_2$  is also observed in solid HD slightly lower at  $1324.9$  and  $1285.8\text{ cm}^{-1}$ , which in this case arises because of isotopic exchange leaving behind a  $D_2$  ligand,  $GdH_2(D_2)$ . Similar isotopic rearrangements between classical and nonclassical hydride positions have been observed in other such complexes.<sup>6,8</sup> Clearly, a weak dihydrogen complex is formed with  $GdH_2$  in solid hydrogen, but our calculations find that the binding of  $H_2$  to  $GdH_2$  is very weak, and we cannot determine the number of such  $H_2$  ligands. We do, however, associate the  $3385\text{ cm}^{-1}$  band and the much stronger deuterium counterpart at  $2441\text{ cm}^{-1}$  (H/D ratio 1.3867) with the strongest of such H–H stretching modes of this

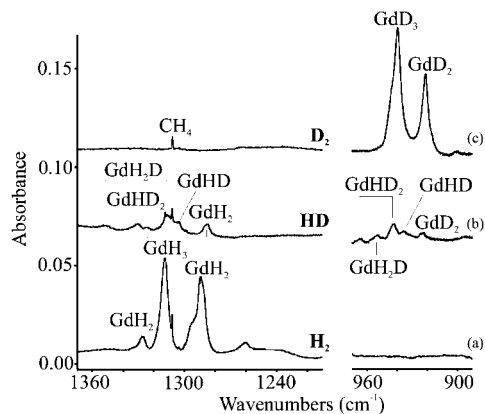


**Figure 5.** Infrared spectra for the major Gd atom reaction products with isotopic molecular hydrogen samples during codeposition at 4 K. (a) H<sub>2</sub>, (b) HD, and (c) D<sub>2</sub>. The labels identify the core isotopic molecules in larger complexes. In the HD experiment, the GdH<sub>2</sub>(D<sub>2</sub>) and GdD<sub>2</sub>(H<sub>2</sub>) complexes are implicated through isotopic positional exchange.

GdH<sub>2</sub>(HH)<sub>x</sub> complex. Second, the strong GdH<sub>3</sub> antisymmetric Gd–H stretching mode at 1312.9 cm<sup>-1</sup> is near our calculated 1296 cm<sup>-1</sup> value, which is satisfactory considering all of the approximations involved. The GdH<sub>2</sub>D isotopic modification will then have an antisymmetric GdH<sub>2</sub> mode near that of GdH<sub>3</sub> (the 1311.3 cm<sup>-1</sup> band in solid HD is identified accordingly) and a higher-frequency symmetric GdH<sub>2</sub> stretching counterpart (because the weaker nondegenerate mode for GdH<sub>3</sub> is computed to be higher than the degenerate mode), and the 1351.8 cm<sup>-1</sup> band fits. The nearly median band at 1330.9 cm<sup>-1</sup> is then due to the single Gd–H stretching mode of GdHD<sub>2</sub>. In solid D<sub>2</sub>, the GdD<sub>2</sub> molecule is observed at 921.5 cm<sup>-1</sup>, and the GdHD(HD) band is observed at 936.2 cm<sup>-1</sup> in solid HD. The degenerate mode of GdD<sub>3</sub> is at 939.9 cm<sup>-1</sup> in solid D<sub>2</sub>, and the antisymmetric Gd–D mode of GdHD<sub>2</sub> is at 943.2 cm<sup>-1</sup> with the symmetric counterpart at 964.8 cm<sup>-1</sup> in solid HD. The intermediate band at 953.8 cm<sup>-1</sup> is the Gd–D stretching mode of GdH<sub>2</sub>D. Therefore, in solid HD, we observed three stretching modes for each of the two mixed isotopic core molecules GdH<sub>2</sub>D and GdHD<sub>2</sub>, which confirms their identification as trihydride core molecules. Isotopic substitution, isotopic frequency calculations, and previous work<sup>5</sup> support this conclusive isotopic identification of the trihydride species.

Notice next that the 3 bands increase on light irradiation, whereas the 2 bands decrease. This enables us to associate weak H–H stretching modes near 3900 cm<sup>-1</sup> with the trihydride complex and stronger such bands in the 3400–3600 cm<sup>-1</sup> region with the dihydride complexes. We note that the H/D ratios of these two distinctly different H–H stretching absorptions are also different, with the higher bands near 1.389 and the lower bands near 1.375 and 1.365 for the two in Figure 3a. The more strongly bound and more red-shifted H–H stretching modes are often more anharmonic, as indicated by the lower H/D isotopic frequency ratios. This may suggest that LnH<sub>3</sub> binds H<sub>2</sub> more weakly than LnH<sub>2</sub>, even if the energy differences are small.

The 1233.7 cm<sup>-1</sup> peak in the Ce experiment increases upon irradiation and is assigned to the CeH<sub>3</sub>(H<sub>2</sub>)<sub>y</sub> complex, which is in accord with the present computations. The 1224.6 cm<sup>-1</sup> peak that decreases on irradiation is then attributed to the CeH<sub>2</sub>(H<sub>2</sub>)<sub>y</sub> complex, which follows our calculations and the previous 1282 cm<sup>-1</sup> solid argon identification.<sup>5</sup> We repeated these argon matrix experiments including HD and D<sub>2</sub> substitution and reaffirm the CeH<sub>2</sub> assignment but not the CeH<sub>3</sub> assignment.<sup>5</sup> The 3662 and 3409 cm<sup>-1</sup> bands (labeled 2 in Figure 3) have HD and D<sub>2</sub>

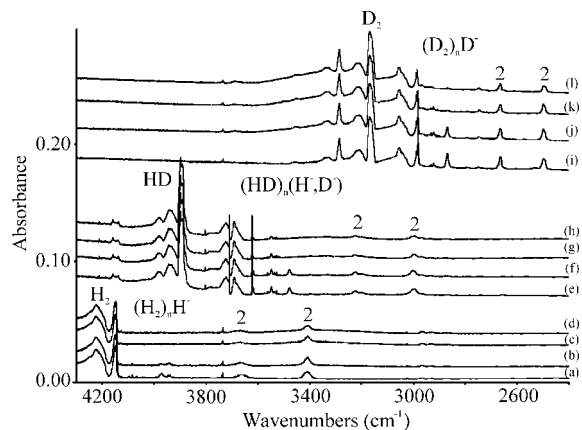


**Figure 6.** Infrared spectra for the Ce atom reaction product with isotopic molecular hydrogens. (a) Co deposition with H<sub>2</sub>, (b) after >320 nm irradiation, (c) after >290 nm irradiation, and (d) after annealing to 6.5 K; (e) Codeposition with HD, (f) after >470 nm irradiation, (g) after >290 nm irradiation, and (h) after annealing to 8 K; and (i) Codeposition with D<sub>2</sub>, (j) after 630 nm irradiation, (k) after >290 nm irradiation, and (l) after >220 nm irradiation.

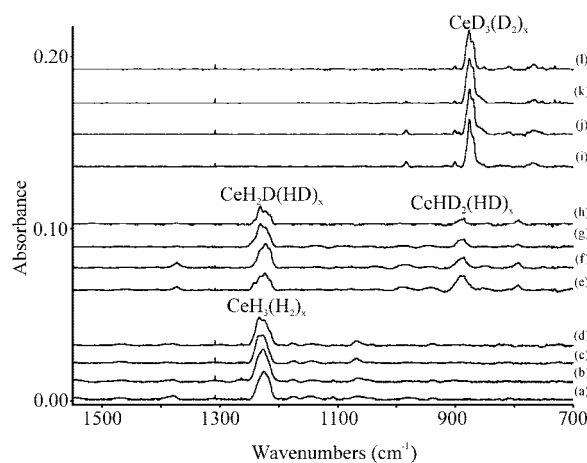


**Figure 7.** Infrared spectra for the Ce atom reaction product with isotopic molecular hydrogens. (a) Co deposition with H<sub>2</sub>, (b) after >320 nm irradiation, (c) after >290 nm irradiation, and (d) after annealing to 6.5 K; (e) Codeposition with HD, (f) after >470 nm irradiation, (g) after >290 nm irradiation, and (h) after annealing to 8 K; and (i) Codeposition with D<sub>2</sub>, (j) after 630 nm irradiation, (k) after >290 nm irradiation, and (l) after >220 nm irradiation.

counterparts at 3222 and 2998 cm<sup>-1</sup> and at 2664 and 2497 cm<sup>-1</sup> in Figure 6 (H/D ratios 1.3746 and 1.3652). These are clearly due to H<sub>2</sub> (HD or D<sub>2</sub>) ligand stretching modes. Figure 7 shows the Ce–H and Ce–D stretching regions of the spectra. Figure S1 in the Supporting Information compares spectra for the Ce reaction with *para*-hydrogen and *ortho*-deuterium. Finally, the two 1265.6 and 1232.9 cm<sup>-1</sup> bands using Pr have the analogous PrH<sub>3</sub>(HH)<sub>y</sub> and PrH<sub>2</sub>(HH)<sub>y</sub> assignments following the 1286 cm<sup>-1</sup> attribution to PrH<sub>2</sub> in solid argon.

The strong 1269.5 cm<sup>-1</sup> band observed here for NdH<sub>3</sub> in solid hydrogen is in line with the present calculation of strong bands at 1310 and 1324 cm<sup>-1</sup> for this molecule, and both show that the earlier 1150 cm<sup>-1</sup> assignment<sup>5</sup> is not correct. The H/D = 1269.5/908.7 = 1.397 ratio is appropriate for an Nd–H stretching mode. Furthermore, the present HD experiment reveals the three band patterns at 1268.0, 1291.0, and 1313.5 cm<sup>-1</sup> and at 913.7, 925.7, 937.5 cm<sup>-1</sup> for the six absorptions of NdH<sub>2</sub>D and NdHD<sub>2</sub> analogous to those discussed above for the Gd species. Therefore, we are confident that the strong 1269.5 cm<sup>-1</sup> band is due to the NdH<sub>3</sub> core molecule in solid

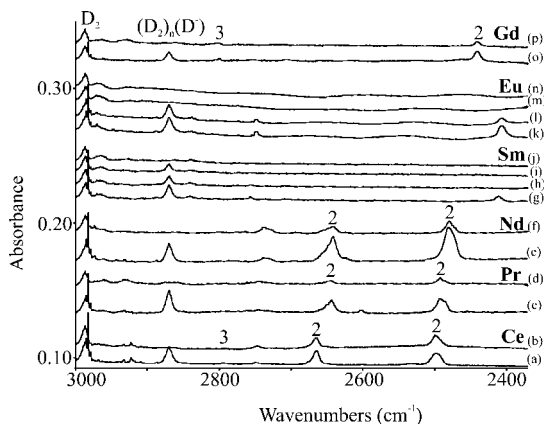


**Figure 8.** Infrared spectra for the products of reaction of early lanthanide metal atoms with dideuterium during co-condensation at 4 K. (a) Ce codeposition, (b) after >290 nm irradiation; (c) Pr codeposition, (d) after 240–380 nm irradiation; (e) Nd codeposition, (f) after 240–380 nm irradiation; (g) Sm codeposition, (h) after >680 nm irradiation, (i) after 530 nm irradiation, and (j) after 240–380 nm irradiation; (k) Eu codeposition, (l) after >680 nm irradiation, (m) after 240–380 nm irradiation, and (n) after >220 nm irradiation; and (o) Gd codeposition, and (p) after 240–380 nm irradiation.

hydrogen. The weaker band at  $1230.2\text{ cm}^{-1}$  is assigned to  $\text{NdH}_2(\text{H}_2)_y$ , which is higher than the previous argon matrix assignment to  $\text{NdH}_2$ .<sup>5</sup> We repeated these argon matrix experiments at 5 K and reaffirm the  $1148\text{ cm}^{-1}$  assignment to  $\text{NdH}_2$  including HD and  $\text{D}_2$  substitution, as discussed by Willson and Andrews.<sup>5</sup>

The  $1291.1\text{ cm}^{-1}$   $\text{SmH}_3$  core band is increased five fold on >470 nm visible irradiation, which destroys a sharp  $1197.7\text{ cm}^{-1}$  absorption. Our calculations predict a strong  $1243\text{ cm}^{-1}$  harmonic fundamental for the octet ground-state  $\text{SmH}$ , and the sharp  $1197.7\text{ cm}^{-1}$  band (H/D ratio 1.402) is appropriate for  $\text{SmH}$ , of course in the  $\text{SmH}(\text{H}_2)_y$  complex. Next, 240–380 nm ultraviolet irradiation almost removes the  $1291.1\text{ cm}^{-1}$  band and restores some of the  $\text{SmH}$  signal, and subsequent visible irradiation of >530 nm reverses this process (Figure 4g–j). Therefore, the  $\text{SmH} + \text{H}_2 \rightarrow \text{SmH}_3$  reaction is reversible with vis–UV irradiation. In addition, the  $\text{SmH}_3$  identification is confirmed with mixed H and D species as bands observed at  $1291.1$ ,  $1311.8$ , and  $1335.5\text{ cm}^{-1}$  and at  $927.8$ ,  $940.1$ , and  $951.9\text{ cm}^{-1}$  for  $\text{SmH}_2\text{D}$  and  $\text{SmHD}_2$ , as described above for the Gd species. Finally, the  $1113.6\text{ cm}^{-1}$  band is assigned to the antisymmetric  $\text{Sm–H}$  stretching mode in  $\text{SmH}_2$ , which is lower than the  $1156.5\text{ cm}^{-1}$  band so assigned in solid argon<sup>5</sup> owing to complex formation. Our calculated  $1194\text{ cm}^{-1}$  fundamental for the septet state  $\text{SmH}_2$  and its red shift in complexes are supportive; however, our calculation for  $\text{SmH}_3$  finds a planar molecule with  $1125$ ,  $1175$ , and  $1277\text{ cm}^{-1}$  frequencies. Fortunately, complexation with  $\text{H}_2$  tends to increase and coalesce the frequencies ( $1220$ ,  $1239$ , and  $1252\text{ cm}^{-1}$  for the bis complex), so our observation of a strong  $1291\text{ cm}^{-1}$  band for  $\text{SmH}_3(\text{H}_2)_y$  in solid hydrogen is reasonable.

The spectra of Sm and Eu in solid deuterium (Figures 8 and 9) reveal new photosensitive D–D stretching bands at  $2411$  and  $2406\text{ cm}^{-1}$  that track with no other bands in these experiments, and the H–H counterparts are too weak to be observed in solid hydrogen. We performed calculations for metal atom complexes with dihydrogen and found reasonable agreement in the case of Sm and Eu, but for all other early lanthanide metals, these calculations do not match the observed bands. In the case of Ce, Pr, Nd, and Gd, the observed H–H stretching

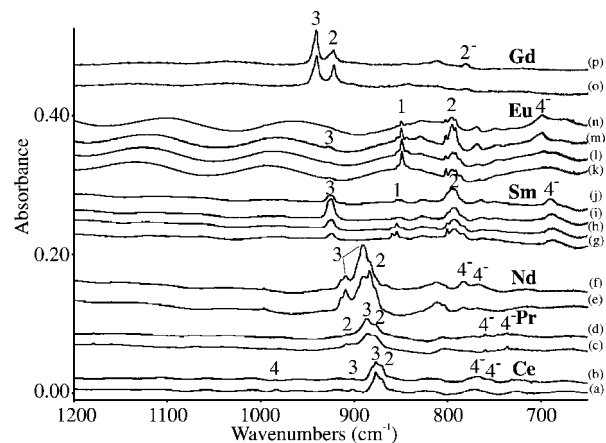


**Figure 9.** Infrared spectra for the products of reaction of early lanthanide metal atoms with dideuterium during co-condensation at 4 K. (a) Ce codeposition, (b) after >290 nm irradiation; (c) Pr codeposition, (d) after 240–380 nm irradiation; (e) Nd codeposition, (f) after 240–380 nm irradiation; (g) Sm codeposition, (h) after >680 nm irradiation, (i) after 530 nm irradiation, and (j) after 240–380 nm irradiation; (k) Eu codeposition, (l) after >680 nm irradiation, (m) after 240–380 nm irradiation, and (n) after >220 nm irradiation; and (o) Gd codeposition, and (p) after 240–380 nm irradiation.

**TABLE 4: Bonding Decomposition Scheme for the Lanthanide and Group VI Atoms, Including Uranium<sup>a</sup>**

|                              | La     | Ce     | Pr     | Nd    | Sm    | Eu    |
|------------------------------|--------|--------|--------|-------|-------|-------|
| prep $\text{MH}_2$           | 1.0    | 0.4    | 0.9    | 0.5   | 3.0   | 0.7   |
| prep $(\text{H}_2)_4$        | 4.5    | 5.7    | 4.9    | 4.7   | 3.8   | 3.7   |
| interaction                  | -26.6  | -26.9  | -20.6  | -19.0 | -17.3 | -13.1 |
| $\text{MH}_2-(\text{H}_2)_4$ |        |        |        |       |       |       |
| total int energy             | -21.2  | -20.9  | -14.8  | -12.9 | -10.5 | -8.8  |
|                              | Cr     | Mo     | W      | Nd    | U     |       |
| prep $\text{MH}_4$           | 0.0    | 36.0   | 24.5   | 4.1   | 2.1   |       |
| prep $(\text{H}_2)_4$        | 77.4   | 21.6   | 24.4   | 8.0   | 6.4   |       |
| interaction                  | -124.0 | -123.9 | -118.0 | -30.5 | -37.8 |       |
| $\text{MH}_4-(\text{H}_2)_4$ |        |        |        |       |       |       |
| total int energy             | -46.6  | -66.3  | -69.1  | -18.3 | -29.3 |       |

<sup>a</sup> Supermolecule has been decomposed in two fragments, the  $\text{MH}_2$  and  $(\text{H}_2)_4$ . In the case of Cr, the decomposition is between Cr and  $(\text{H}_2)_6$ . As mentioned in the text, we could find only a higher energy state for the  $\text{NdH}_4(\text{H}_2)_4$ , but for the purpose of analysis, we have used it in the discussion.

modes track with Ln–H stretching absorptions and agree best with the  $\text{LnH}_2(\text{H}_2)_y$  model.

In the europium spectrum, the  $\text{EuH}$  band is very photosensitive, but a clear relationship with  $\text{EuH}_2$  is not obvious. The sharp  $1189.4$  and structured  $1112.7\text{ cm}^{-1}$  features are both substantially decreased by >470 nm irradiation, but >380 nm exposure restores some of the latter, whereas continued 240–380 nm irradiation decreases the latter and slightly increases the former absorptions. The sharp  $1189.4\text{ cm}^{-1}$  band is assigned here to the ground-state  $\text{EuH}$  molecule (H/D isotopic frequency ratio 1.402), whereas our calculation finds  $1208\text{ cm}^{-1}$  for the nonet ground state. The  $1112.7\text{ cm}^{-1}$  feature (H/D ratio 1.400) arises from the antisymmetric  $\text{EuH}$  stretching mode of the  $\text{EuH}_2$  core molecule observed at  $1155.6\text{ cm}^{-1}$  in solid argon<sup>5</sup> and is computed here as  $1207\text{ cm}^{-1}$ . Again, mixed isotopic data are confirming because the HD experiment gives  $1144.1$  and  $817.5\text{ cm}^{-1}$  bands for the  $\text{EuHD}$  core molecule and bands at  $1114.5$  and  $799.7\text{ cm}^{-1}$  for  $\text{EuH}_2$  and  $\text{EuD}_2$  core species from isotopic exchange in the  $\text{EuHD}(\text{HD})_y$  complexes.

There is a weak  $926\text{ cm}^{-1}$  product of the Eu reaction in solid deuterium, which increases upon photolysis with  $\text{EuD}_2$  at the

**TABLE 5: Natural Population Charges and Natural Electronic Configurations Computed at DFT/BP86/TZVPP Level of Theory for the Lanthanide and Group VI Atoms, Including Uranium, in Different Molecular Fragments<sup>a</sup>**

| molecular system                               | La                                    | Ce   | Pr   | Nd   | Sm   | Eu   | Gd   |
|--|---------------------------------------|--|--|--|--|--|--|
| M  | 5d <sup>1</sup> 6s <sup>2</sup>       | 4f <sup>1</sup> 5d <sup>1</sup> 6s <sup>2</sup>          | 4f <sup>3</sup> 5d <sup>0</sup> 6s <sup>2</sup>          | 4f <sup>4</sup> 5d <sup>0</sup> 6s <sup>2</sup>          | 4f <sup>6</sup> 5d <sup>0</sup> 6s <sup>2</sup>          | 4f <sup>7</sup> 5d <sup>0</sup> 6s <sup>2</sup>          | 4f <sup>7</sup> 5d <sup>1</sup> 6s <sup>2</sup>          |
| MH <sub>2</sub>                                | 5d <sup>1.33</sup> 6s <sup>0.24</sup> | 4f <sup>1.35</sup> 5d <sup>0.60</sup> 6s <sup>0.78</sup> | 4f <sup>2.65</sup> 5d <sup>0.41</sup> 6s <sup>0.69</sup> | 4f <sup>3.85</sup> 5d <sup>0.34</sup> 6s <sup>0.61</sup> | 4f <sup>6.05</sup> 5d <sup>0.24</sup> 6s <sup>0.46</sup> | 4f <sup>7.05</sup> 5d <sup>0.22</sup> 6s <sup>0.49</sup> | 4f <sup>7.05</sup> 5d <sup>0.47</sup> 6s <sup>1.09</sup> |
| charge   | 1.39                                  | 1.29   | 1.29   | 1.29   | 1.34   | 1.33   | 1.40   |
| MH <sub>2</sub> (H <sub>2</sub> ) <sub>4</sub> | 5d <sup>0.95</sup> 6s <sup>0.15</sup> | 4f <sup>1.25</sup> 5d <sup>0.85</sup> 6s <sup>0.15</sup> | 4f <sup>2.5</sup> 5d <sup>0.61</sup> 6s <sup>0.16</sup>  | 4f <sup>3.85</sup> 5d <sup>0.40</sup> 6s <sup>0.18</sup> | 4f <sup>5.95</sup> 5d <sup>0.33</sup> 6s <sup>0.19</sup> | 4f <sup>7.05</sup> 5d <sup>0.29</sup> 6s <sup>0.19</sup> |  |
| charge   | 1.85                                  | 1.76   | 1.71   | 1.63   | 1.60   | 1.58   |  |
|  | Cr                                    | Mo   | W  | Nd   | U  |  |  |
| M  |                                       | 4d <sup>5</sup> 5s <sup>1</sup>                          | 5d <sup>4</sup> 6s <sup>2</sup>                          | 4f <sup>4</sup> 5d <sup>0</sup> 6s <sup>2</sup>          | 5f <sup>3</sup> 6d <sup>1</sup> 7s <sup>2</sup>          |  |  |
| MH <sub>4</sub>                                |                                       | 4d <sup>4.7</sup> 5s <sup>0.8</sup>                      | 5d <sup>4.3</sup> 6s <sup>0.8</sup>                      | 4f <sup>3.35</sup> 5d <sup>0.5</sup> 6s <sup>0.5</sup>   | 5f <sup>2.4</sup> 6d <sup>0.6</sup> 7s <sup>0.1</sup>    |  |  |
| charge   |                                       | 0.56   | 0.72   | 1.86   | 2.91   |  |  |
| MH <sub>4</sub> (H <sub>2</sub> ) <sub>4</sub> |                                       | 4d <sup>6.7</sup> 5s <sup>0.5</sup>                      | 5d <sup>4.5</sup> 6s <sup>0.56</sup>                     | 4f <sup>3.35</sup> 5d <sup>0.57</sup> 6s <sup>0.21</sup> | 5f <sup>2.4</sup> 6d <sup>0.7</sup> 7s <sup>0.01</sup>   |  |  |
| charge   | -1.71                                 | -1.23  | -1.02  | 1.94   | 2.91   |  |  |

<sup>a</sup> Only the major contributions are shown in the table.

**TABLE 6: Total Amount of Charge Transferred from the MH<sub>x</sub> [x = 2, 4] Moiety to the (H<sub>2</sub>)<sub>4</sub> Fragment in the Supermolecule Computed with a Natural Population Analysis at DFT/BP86/TZVPP Level of Theory**

| molecular System                               | La   | Ce   | Pr   | Nd   | Sm   | Eu   | Gd |
|--|------|------|------|------|------|------|----|
| MH <sub>2</sub> (H <sub>2</sub> ) <sub>4</sub> | 0.52 | 0.55 | 0.47 | 0.38 | 0.33 | 0.29 |    |
|  | Cr   | Mo   | W    | Nd   | U    |      |    |
| MH <sub>4</sub> (H <sub>2</sub> ) <sub>4</sub> |      | 1.14 | 1.11 | 0.34 | 0.50 |      |    |

expense of EuD (Figure 9). This weak 926 cm<sup>-1</sup> band with Eu behaves just like the 924 cm<sup>-1</sup> SmD<sub>3</sub> absorption, and we believe that the 926 cm<sup>-1</sup> band is due to the EuD<sub>3</sub> core molecule made from the EuD + D<sub>2</sub> reaction. Therefore, EuD<sub>3</sub>(D<sub>2</sub>)<sub>y</sub> is stabilized by lower ZPE relative to the corresponding EuH<sub>3</sub> complex, which is not observed here.

The spectra in Figures 3 and 4 are concluded with GdH<sub>3</sub> discussed above with the addition of the weak H–H stretching mode at 3888 cm<sup>-1</sup> that is assigned to the GdH<sub>3</sub>(H<sub>2</sub>)<sub>y</sub> complex. This and the counterpart bands at 3894 cm<sup>-1</sup> for SmH<sub>3</sub>(H<sub>2</sub>)<sub>y</sub> and at 3904 cm<sup>-1</sup> for NdH<sub>3</sub>(H<sub>2</sub>)<sub>y</sub> show that the trihydrides bind dihydrogen more weakly than the dihydrides, which give rise to more intense H–H stretching modes in the 3400–3600 cm<sup>-1</sup> region.

In the previous experiments with La and H<sub>2</sub> in excess argon, a new band was observed at 1114 cm<sup>-1</sup>, which increased upon annealing and upon photolysis. Assignment to the antisymmetric stretching mode in LaH<sub>4</sub><sup>-</sup> was substantiated by HD and D<sub>2</sub> substitution and an even stronger band at 1227 cm<sup>-1</sup> for the corresponding YH<sub>4</sub><sup>-</sup> anion.<sup>6,24</sup> An absorption for LaH<sub>4</sub><sup>-</sup> was observed at 1102 cm<sup>-1</sup> in solid neon, which is listed for La in Table 7. Weak bands were observed for the early Ln metal reactions in solid hydrogen in the 970–1100 cm<sup>-1</sup> region, which also exhibited slight increases upon photolysis and early annealing (Table 7, labeled 4<sup>-</sup> in Figure 4). These bands also shifted with solid deuterium as expected for Ln–H/D stretching modes (Figure 9). For example, the two peaks with Ce at 1067 and 1045 cm<sup>-1</sup> shifted to 766 and 753 cm<sup>-1</sup> with deuterium (H/D ratios 1.393, 1.388). In addition the bands are better resolved with Pr at 1072 and 1044 cm<sup>-1</sup> and with Nd at 1091 and 1054 cm<sup>-1</sup>. Calculations predicted an extremely strong triply degenerate mode for CeH<sub>4</sub><sup>-</sup> at 1124 to 1127 cm<sup>-1</sup> (intensity 1245 km/mol × 3) and likewise for PrH<sub>4</sub><sup>-</sup> at about 10 cm<sup>-1</sup> lower and for SmH<sub>4</sub><sup>-</sup> at another 90 cm<sup>-1</sup> lower, which supports the identification of these bands as tetrahydride anions. The absorptions for Ce, Pr, and Nd reactions were split by the hydrogen matrix into two bands (the Ce product bands are better resolved in *para*-hydrogen and *ortho*-deuterium, Figure S1 in the Supporting Information), but only a single band was

**TABLE 7: Infrared Absorptions (cm<sup>-1</sup>) Observed for Early Lanthanide Metal Atom Reaction Products with Pure Hydrogen (Top List) or Deuterium (Bottom List) at 4 K<sup>a</sup>**

| La | Ce             | Ce( <i>p</i> -H <sub>2</sub> ) | Pr    | Nd             | Sm             | Eu             | Gd             | ident                       |
|----|----------------|--------------------------------|-------|----------------|----------------|----------------|----------------|-----------------------------|
|    | 3801<br>[3654] |                                |       |                | 3894<br>[3704] |                | 3888<br>[3720] | 3                           |
|    | 3685<br>[3710] | 3662<br>[3613]                 | 3655  | 3632<br>[3670] | 3672<br>[3741] |                |                | 2                           |
|    | 3409<br>[3520] | 3409<br>[3426]                 | 3401  | 3398<br>[3593] | 3380<br>[3538] |                | 3385<br>[3417] | 2                           |
|    |                | 1381<br>[1346]                 |       |                |                |                |                | 4                           |
|    |                | 1262<br>[1234]                 | 1264  | 1302<br>[1241] |                |                | 1327<br>[1288] | 3                           |
|    |                | 1256<br>[1250]                 | 1258  |                |                |                |                | 2                           |
|    | 1214<br>[1234] | 1234<br>[1232]                 | 1236  | 1266<br>[1236] | 1270<br>[1200] | 1291           | 1313<br>[1279] | 3                           |
|    |                | 1225<br>[1236]                 | 1226  | 1233<br>[1223] | 1230<br>[1205] | 1114<br>[1168] | 1112<br>[1167] | 2                           |
|    |                | 1108                           | 1108  | 1149           |                |                | 1201           | ?                           |
|    |                |                                |       |                | 1198<br>[1243] | 1189<br>[1208] |                | 1                           |
|    | 1102<br>[1124] | 1067<br>[1125]                 | 1069  | 1072<br>[1120] | 1091<br>[1110] | 1020<br>[1020] | 990<br>[990]   | 1083 <sup>b</sup><br>[1079] |
|    |                | 1045<br>[1125]                 | 1042  | 1044<br>[1114] | 1054<br>[1110] | 976<br>[1037]  | 987<br>[1003]  | 4 <sup>-</sup>              |
|    |                |                                |       |                |                |                |                | Deuterated Species          |
|    | 2747           | 2746 <sup>c</sup>              |       |                |                |                | 2799           | 3                           |
|    | 2681           | 2664                           | 2660  | 2643           | 2642           |                |                | 2                           |
|    | 2466           | 2497                           | 2487  | 2485           | 2479           |                | 2441           | 2                           |
|    |                | 983                            | 983   |                |                | 2411           | 2406           | M(DD) <sub>2</sub>          |
|    |                | 900                            | 902.6 |                |                |                | 976            | 4                           |
|    |                | 893                            | 895.3 | 909            |                |                |                | 3                           |
|    | 864            | 876                            | 878.5 | 887            | 908.7          | 924.1          | 926            | 2                           |
|    |                | 869                            | 871.9 | 875            | 883.2          | 793.5          | 790.9          | 939.9                       |
|    |                |                                | 792.5 |                | 811            |                |                | 921.5                       |
|    |                |                                |       |                |                | 854.3          | 848.5          | 892.6                       |
|    |                |                                |       |                |                |                |                | ?                           |
|    | 783            | 766                            | 766   | 760            | 783            |                |                | 1                           |
|    |                | 753                            | 754   | 737            | 770            | 690            | 699            | 780 <sup>b</sup>            |
|    |                |                                |       |                |                |                |                | 4 <sup>-</sup>              |

<sup>a</sup> Computed vibrational frequencies (cm<sup>-1</sup>) at DFT/BP86/TZVPP level of theory for all of the species are given in brackets. For simplicity, we give just the frequencies for the supercomplexes with six H<sub>2</sub> molecules for La, Ce, Nd, and Sm and with four H<sub>2</sub> molecules for Eu and Gd. A complete survey of all computed frequencies for all species is given in the Supporting Information. The last column, ident, stands for the number of x hydrogen atoms in the binary MH<sub>x</sub> complex. A question mark, ?, means that the number x could not be identified. <sup>b</sup> These bands are assigned to the dihydride anion. <sup>c</sup> This and bands below from Ce and *o*-D<sub>2</sub> reaction.

observed for Sm and Eu. These molecular anions are probably formed here through H<sup>-</sup> capture by the trihydride molecule (reaction exothermic by 70–80 kcal/mol), except in the case of Eu where the reaction probably involves the dihydride, H<sub>2</sub>, and H<sup>-</sup>. Note, however, that the EuD<sub>4</sub><sup>-</sup> band is substantially



stronger than the  $\text{EuH}_4^-$  absorption (compare the spectra in Figures 8 and 9), and this is in accord with the zero-point stabilization of the deuterated species and the observation of  $\text{EuD}_3$ . (See above.) We note that the tetrahydride anion absorptions are relatively stronger in the group III metal reaction systems<sup>6,24</sup> than with the early lanthanide metals. However, the reaction exothermicity is greater and the metal hydride bonds are shorter for the lanthanide tetrahydride anions, which follows the principle of lanthanide contraction. The present definitive identification of  $\text{SmH}$  and  $\text{EuH}$  with 1198 and 1189  $\text{cm}^{-1}$  fundamentals in solid hydrogen having little matrix interaction provides an experimental basis to support the  $\text{SmH}$  octet  $[(4f^6)(6s)](\sigma, 6s-1s)^2$  and  $\text{EuH}$  nonet  $[(4f^7)(6s)](\sigma, 6s-1s)^2$  ground-state electronic configurations from our DFT calculations, which were predicted earlier by Dolg and Stoll.<sup>25</sup> These solid hydrogen matrix observations may assist in the eventual observation of the gas-phase spectrum. Finally, the single band observed for Gd at 1083  $\text{cm}^{-1}$  and that for the deuterium counterpart at 780  $\text{cm}^{-1}$  (H/D ratio 1.388) decrease 30% upon UV irradiation, and these bands are appropriate for  $\text{GdH}_2^-$  and  $\text{GdD}_2^-$  because our calculations show that the tetrahydride anion disproportionates to the dihydride anion with frequencies in this region.

**Bond Analysis.** To understand how different metals interact with H and  $\text{H}_2$ , we have analyzed the stability of various  $\text{MH}_x(\text{H}_2)_y$  [ $x = 2, 3, 4; y = 1, \dots, 6$ ] clusters. Such a stability can be expressed as the difference between the total energy (including ZPE) of the complexes and the energy of their components, namely,  $\text{MH}_x$  and  $y\text{H}_2$ . The total interaction energy term can be decomposed in several contributions, as shown in Table 4 and as explained in the Computational and Experimental Methods section. For simplicity, in the analysis, we will consider only the  $\text{MH}_2(\text{H}_2)_4$  supercomplexes for the lanthanide series and the  $\text{MH}_4(\text{H}_2)_4$  complexes for the group VI series and for Nd and U. We decided to focus on the systems with four  $\text{H}_2$  molecules because this is the largest number of  $\text{H}_2$  that can bind the  $\text{WH}_4$  and  $\text{MoH}_4$  species. As for the nomenclature, we will use  $y\text{H}_2$  to indicate the number of isolated  $\text{H}_2$ , whereas  $(\text{H}_2)_y$  is referred to as the  $y$   $\text{H}_2$  molecules in the supercomplex.

When forming the  $\text{MH}_x(\text{H}_2)_y$  supercomplex, a substantial charge transfer between  $\text{MH}_x$  and  $(\text{H}_2)_y$  occurs. However, to make our model simpler, we assume that the strain energy term includes only the effect of the geometrical distortion. In other words, we assume that  $\text{MH}_x$  and  $(\text{H}_2)_y$  have the same electronic configuration in the supercomplex and as isolated species. In such a way, all of the electronic effects are included in the interaction energy term.

In regards to the lanthanide series, we notice that the total interaction energy decreases going from La to Eu, as shown in Table 3. Neither the  $\text{MH}_2$  moiety nor the  $4\text{H}_2$  molecules undergo any major deformation when they form the supercomplex. The effect of putting four  $\text{H}_2$  molecules close to each other, as they appear in the supercomplex  $\text{MH}_2(\text{H}_2)_4$ , is only a small destabilization that ranges between 4 and 6 kcal/mol. The preparation energy of  $\text{MH}_2$  is almost negligible, about 0.5 to 1.0 kcal/mol. The most significant term that explains the trend of total binding energy is the local interaction between  $\text{MH}_2$  and  $(\text{H}_2)_4$ . To understand it, in Table 5, we report the natural electronic configurations of the metal atoms in  $\text{MH}_2(\text{H}_2)_4$  and in the isolated  $\text{MH}_2$  molecules. In the latter, the hydrogen atoms behave as the electron attractor, and the lanthanide atom behaves as the electron donor. This is the consequence of a depletion of the 6s orbital on the metal that mainly donates its charge to the 1s orbitals on the hydrogen atoms. A further reorganization

occurs on the metal with polarization effects within the 6s, 5d, and 4f orbitals. The total charge on the lanthanide elements in  $\text{MH}_2$  varies in the range of +1.39 (La) to +1.29 (Ce, Pr, Nd). In the supercomplexes,  $\text{MH}_2(\text{H}_2)_4$ , the metal bears an overall larger positive charge than that in the  $\text{MH}_2$  species, and the charge variation along the series is also larger: from +1.85 in La to +1.58 in Eu. This means that some charge transfer occurs from the  $\text{MH}_2$  moiety to the  $(\text{H}_2)_4$  fragment and that the heavier the metal the less it participates in this new type of bonding. An inspection of the natural electronic configurations reported in Table 4 helps us to understand this effect. In going from  $\text{MH}_2$  to  $\text{MH}_2(\text{H}_2)_4$ , the Ce 6s orbital is depleted of about 0.63e, whereas the Eu 6s orbital is depleted of only 0.30e. Part of this charge goes to the 5d orbitals through polarization induced by the  $\text{H}_2$  molecules, whereas the remaining charge is back-donated to the empty antibonding orbitals of the  $\text{H}_2$ . The 4f orbitals are corelike and act as spectators. This trend is further confirmed when we compute the net charge transfer between the two fragments, as summarized in Table 5.

The behavior is different for group VI elements. The inspection of the preparation energy terms reported in Table 3 indicates that both  $\text{MH}_4$  and  $(\text{H}_2)_4$  are strongly deformed with respect to the lanthanide (and also actinide) elements. For  $\text{MoH}_4$  and  $\text{WH}_4$ , the preparation energy is equal to 36.0 and 24.5 kcal/mol, respectively. A similar amount of energy is required as preparation energy for  $(\text{H}_2)_4$ . The interaction energies are strongly stabilizing and about five times larger than those in the lanthanide series. Because of the large deformation of the fragments, the final bonding energy is three times larger than that in the lanthanide case. By looking at the structures (Figure 2), we already notice that the orientation of the four  $\text{H}_2$  molecules in  $\text{MoH}_4(\text{H}_2)_4$  and  $\text{WH}_4(\text{H}_2)_4$ , is different compared with the orientation in  $\text{NdH}_4(\text{H}_2)_4$  and  $\text{UH}_4(\text{H}_2)_4$ . In the Nd/U case, the  $\text{H}_2$  molecules are positioned in between two adjacent hydrogen atoms of the  $\text{MH}_4$  moiety (Figure 3b), whereas in the Mo/W case, the  $\text{H}_2$  molecules are far from the two hydrogen atoms. To understand this difference, we have to inspect the natural electronic configurations reported in Table 5. It is evident that the 4d (5d) orbitals of Mo(W), unlike in the lanthanide case, are involved directly in the bond with the peripheral  $\text{H}_2$  molecules. The contribution is fairly large. The 4d (5d) orbitals of Mo(W) go from an occupation of 4.7 (4.5) in  $\text{MoH}_4(\text{WH}_4)$  to 6.7 (6.4) in  $\text{MoH}_4(\text{H}_2)_4(\text{WH}_4(\text{H}_2)_4)$ , indicating the favorable energetic match with the occupied  $\sigma$  bonding orbitals of the peripheral  $\text{H}_2$  molecules that act as electron donors. The charge on Mo and W is negative in the supercomplex, -1.23 and -1.02, respectively. The total net transfer between the two fragments is 1.14 for Mo and 1.11 for W, and the charge, unlike in the lanthanide case, floats from the  $\text{MH}_4$  moiety to the  $\text{H}_2$  molecules. One should also notice a depletion of the 5s (Mo) and 6s (W) shell that probably accounts for a small backdonation to the  $(\text{H}_2)_4$  fragment and a concomitant polarization to the 4d (Mo) and 5d (W) shells.

In the chromium case, as already mentioned in the Structures and Energetics section, when  $4\text{H}_2$  molecules are bound to  $\text{CrH}_4$ , the supercomplex transforms during geometry optimization to  $\text{Cr}(\text{H}_2)_6$ . Hence, we performed a bond decomposition by considering Cr as one fragment and  $(\text{H}_2)_6$  as the other fragment. The results are presented Table 4. The preparation of the Cr atom is null, whereas the  $(\text{H}_2)_6$  preparation costs about 77.4 kcal/mol, because of a large Pauli repulsion between the neighboring  $\text{H}_2$  molecules in the supercomplex. Most of the contribution to the total bonding energy comes from the interaction energy term, 124 kcal/mol, a value attributable to

an electron donation that takes place from the sigma bonding of H<sub>2</sub> to the 3d orbitals of Cr.

In summary, for the lanthanide series when the MH<sub>2</sub> molecule binds hydrogen molecules, the 4f electrons behave like core, the empty 5d orbitals do not have a favorable energetic interaction with the occupied H<sub>2</sub> bonding orbitals, and most of the bonding interaction occurs because the 6s electrons on the metal are partially transferred to the empty orbitals of the (H<sub>2</sub>)<sub>4</sub> fragment. NdH<sub>4</sub> and UH<sub>4</sub> follow a similar pattern. For the elements of group VI, the behavior is different, and the d orbitals participate in the bond by withdrawing electrons from the (H<sub>2</sub>)<sub>6</sub> bonding molecular orbitals.

## Conclusions

We have presented the results of a combined spectroscopic and computational study of lanthanide hydrides with the general formula MH<sub>x</sub>(H<sub>2</sub>)<sub>y</sub>, where M = La, Ce, Pr, Nd, Sm, Eu, and Gd, x = 1–4, y = 0–6. Comparative calculations were also performed on the species in which the central metal, M, is Mo, W, and U.

To understand the dihydrogen complexes formed with lanthanide metal hydride molecules, we have first identified the binary MH<sub>x</sub> molecule formed in the ablation/deposition process, which becomes the core of the dihydrogen supercomplex, MH<sub>x</sub>(H<sub>2</sub>)<sub>y</sub>. Our investigation has shown that the trihydrides bind dihydrogen more weakly than the dihydrides, which give rise to more intense H–H stretching modes in the 3400–3600 cm<sup>-1</sup> region. We have observed sharp new absorptions for SmH and EuH and broader absorptions for the MH<sub>4</sub><sup>-</sup> anions in solid hydrogen.

The result of the analysis of the bond between the lanthanide metal is that when the MH<sub>2</sub> molecule binds several hydrogen molecules the 4f electrons behave like core, the empty 5d orbitals do not have a favorable energetic interaction with the occupied H<sub>2</sub> bonding orbitals, and most of the bonding interaction occurs because the 6s electrons on the metal are partially transferred to the empty orbitals of the (H<sub>2</sub>)<sub>4</sub> fragment. The NdH<sub>4</sub> and UH<sub>4</sub> species follow a similar pattern. For the group VI metals, Mo and W, the behavior is different, and the d orbitals participate in the bond by withdrawing electrons from the H<sub>2</sub> bonding molecular orbitals.

**Acknowledgment.** We gratefully acknowledge support for this research from the U.S. National Science Foundation under grant no. CHE03-52487 and the Swiss National Science Foundation (grant no. 200020-120007).

**Supporting Information Available:** Calculated frequencies and geometrical coordinates for all structures and infrared spectra for Ce reactions with *para*-hydrogen and *ortho*-deuterium. This material is available free of charge via the Internet at <http://pubs.acs.org>.

## References and Notes

- (1) Thematic Issue on Hydrogen, *Chem. Rev.* **2007**, *107*, 3899–4435.
- (2) Kubas, G. J.; Ryan, R. R.; Swanson, B. I.; Vergamini, P. J.; Wasserman, H. J. *J. Am. Chem. Soc.* **1984**, *106*, 451–452.
- (3) Kubas, G. J.; Ryan, R. P.; Wroblewski, D. A. *J. Am. Chem. Soc.* **1986**, *108*, 1339–1341.
- (4) Kubas, G. J. In *Modern Inorganic Chemistry*; Fackler, J. P. J., Ed.; Kluwer Academic/Plenum: New York, 2001.
- (5) Willson, S. P.; Andrews, L. *J. Phys. Chem. A* **2000**, *104*, 1640–1647.
- (6) Wang, X. F.; Chertihin, G. V.; Andrews, L. *J. Phys. Chem. A* **2002**, *106*, 9213–9225.
- (7) Wang, X. F.; Andrews, L.; Gagliardi, L. *J. Phys. Chem. A* **2008**, *112*, 1754–1761.
- (8) Wang, X. F.; Andrews, L.; Infante, I.; Gagliardi, L. *J. Am. Chem. Soc.* **2008**, *130*, 1972–1978.
- (9) Gagliardi, L.; Pyykko, P. *J. Am. Chem. Soc.* **2004**, *126*, 15014–15015.
- (10) Raab, J.; Lindh, R. H.; Wang, X. F.; Andrews, L.; Gagliardi, L. *J. Phys. Chem. A* **2007**, *111*, 6383–6387.
- (11) Wang, X. F.; Andrews, L. *J. Am. Chem. Soc.* **2002**, *124*, 5636–5637.
- (12) Wang, X. F.; Andrews, L. *J. Phys. Chem. A* **2003**, *107*, 570–578.
- (13) Wang, X. F.; Andrews, L. *J. Phys. Chem. A* **2005**, *109*, 9021–9027.
- (14) Ahlrichs, R.; Bar, M.; Haser, M.; Horn, H.; Kolmel, C. *Chem. Phys. Lett.* **1989**, *162*, 165–169.
- (15) Cao, X. Y.; Dolg, M. *J. Chem. Phys.* **2001**, *115*, 7348–7355.
- (16) Perdew, J. P.; Burke, K.; Ernzerhof, M. *Phys. Rev. Lett.* **1996**, *77*, 3865–3868.
- (17) Ernzerhof, M.; Scuseria, G. E. *J. Chem. Phys.* **1999**, *110*, 5029–5036.
- (18) Infante, I.; Gagliardi, L.; Scuseria, G. E. *J. Am. Chem. Soc.* **2008**, *130*, 7459–7465.
- (19) Infante, I.; Raab, J.; Lyon, J. T.; Liang, B.; Andrews, L.; Gagliardi, L. *J. Phys. Chem. A* **2007**, *111*, 11966–12000.
- (20) Gagliardi, L.; Heaven, M. C.; Krogh, J. W.; Roos, B. O. *J. Am. Chem. Soc.* **2005**, *127*, 86–91.
- (21) Andrews, L. *Chem. Soc. Rev.* **2004**, *33*, 123–132.
- (22) Silvera, I. F. *Rev. Mod. Phys.* **1980**, *52*, 393–452.
- (23) Andrews, L.; Wang, X. F. *Rev. Sci. Instrum.* **2004**, *75*, 3039–3044.
- (24) Wang, X. F.; Andrews, L. *J. Phys. Chem. A* **2004**, *108*, 1103–1106.
- (25) Dolg, M.; Stoll, H. *Theor. Chim. Acta* **1989**, *75*, 369–387.